THE JOURNAL OF PHYSICAL CHEMISTRY Letters

Letter

pubs.acs.org/JPCL

Lonsdaleite Films with Nanometer Thickness

Alexander G. Kvashnin*[,†,‡] and Pavel B. Sorokin[†,‡,∥]

[†]Technological Institute of Superhard and Novel Carbon Materials, 7a Centralnaya Street, Troitsk, Moscow 142190, Russian Federation

[‡]Moscow Institute of Physics and Technology, 9 Institutsky lane, Dolgoprudny 141700, Russian Federation

[∥]National University of Science and Technology "MISIS", Leninsky Avenue 4, Moscow 119049, Russian Federation

Supporting Information

ABSTRACT: We investigate the properties of potentially the stiffest quasi-2-D films with lonsdaleite structure. Using a combination of ab initio and empirical potential approaches, we analyze the elastic properties of lonsdaleite films in both elastic and inelastic regimes and compare them with graphene and diamond films. We review possible fabrication methods of lonsdaleite films using the pure nanoscale "bottom-up" paradigm: by connecting carbon layers in multilayered graphene. We propose the realization of this method in two ways: by applying direct pressure and by using the recently proposed chemically induced phase transition. For both cases, we construct the phase diagrams depending on temperature, pressure, and film thickness. Finally, we consider the electronic properties of lonsdaleite films and establish the nonlinear dependence of the band gap on the films' thicknesses and their lower effective masses in comparison with bulk crystal.

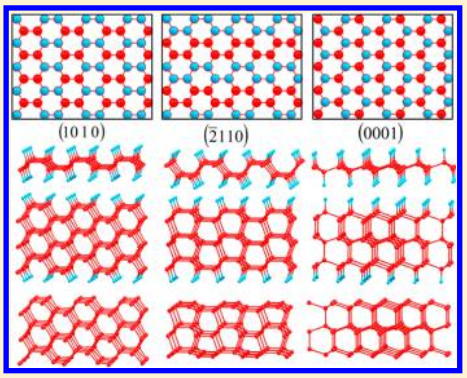

SECTION: Physical Processes in Nanomaterials and Nanostructures

Lonsdaleite is a carbon allotrope with a hexagonal lattice, often called hexagonal diamond due to its crystal structure. Since it was first observed in the Canyon Diablo meteorite by Foote[1] and later by Frondel and Marvin,[2] this phase was identified only as an incorporation in diamond matrix through topological defects such as stacking faults or twin boundaries.[3−5] The fraction of the lonsdaleite phase was usually tiny and only recently was a 50% lonsdaleite found.[6] Hexagonal diamond has never been obtained as a freestanding single crystal. Because of this, lonsdaleite is considered a purely hypothetical object. However, theoretical predictions show the great promise of this structure. Lonsdaleite is simulated to be over 50% harder than diamond on the ⟨100⟩ face and is shown to resist indentation pressures up to 152 GPa. Diamond breaks at only 97 GPa, making lonsdaleite one of the hardest crystals.[7]

Current synthesis methods do not allow us to create lonsdaleite crystals for applications, but the nanoscale "bottom-up" paradigm allows us to fabricate hexagonal diamond films of nanometer thickness from smaller objects such as graphene. We can assume that lonsdaleite nanofilms can be fabricated by the chemical junction of layers in multilayered graphene due to the number of theoretical predictions[8−10] and experimental confirmations[11−13] of the diamondization of multilayered graphene. Graphene layers can be connected by using two different driving forces: direct pressure[13] and the chemical adsorption of adatoms on the multilayer graphene surface.[8−12] The last approach was named "chemically induced phase transition".[14]

The sp^3-hybridized carbon films have drawn a lot of attention due to interesting physical properties. A number of papers were published in recent years with description of their electronic,[8,9,15] magnetic,[16] and elastic[17] properties. Lonsdaleite films of nanometer thickness can also be of interest because they could combine the high elastic constants of bulk crystal with the flexibility and high carrier mobility of thin carbon films.[8] We can also expect that because of their similarity to nanometer-thick diamond films lonsdaleite films will display electronic properties that depend on the film's thickness.

We began our study with analysis of the atomic structure and stability of nanometer thick lonsdaleite films with crystallographic surfaces (10$\bar{1}$0), ($\bar{2}$110), and (0001). We found the critical size at which lonsdaleite film with a clean surface splits into the AA- and AA′-stacked graphene. We then investigated the phase transition from multilayered graphene to lonsdaleite films. The comparison of the ab initio computed Gibbs free energies allowed us to obtain the phase diagram $P(T)$ as a function of film's thickness. We considered the effect of chemically induced phase transition for films with a hydrogenated surface (named diamanes[8]) and found the conditions for when the pressure of phase transition formally turns negative. The mechanical properties of lonsdaleite films were obtained and compared with diamond films with (111) surface. The elastic constants of the films were estimated, and the

Received: November 21, 2013
Accepted: January 5, 2014

   dx.doi.org/10.1021/jz402528q | J. Phys. Chem. Lett. 2014, 5, 541−548

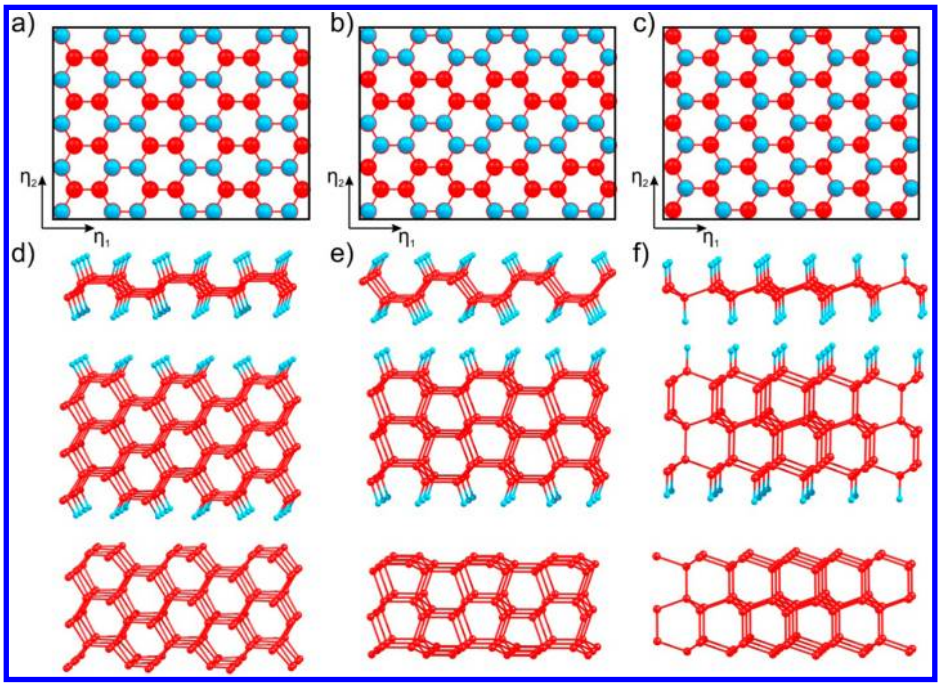

Figure 1. Schematic illustration of the hydrogen coverage of the graphane conformers (a) "boat1", (b) "boat2", and (c) "chair1" showing the atomic structure of the considered graphane conformers and corresponding three-layered lonsdaleite films with hydrogenated and clean surfaces with (d) $(10\bar{1}0)$, (e) $(\bar{2}110)$, and (f) (0001) crystallographic orientations.

behavior of the films under critical strain was investigated. We found that lonsdaleite films are second in stiffness only to bulk lonsdaleite and graphene but display the same flexibility as diamond films. Finally, we studied the electronic properties of films. The band-gap dependence on the thickness of lonsdaleite films was obtained, and its nonlinear behavior was discussed. The carrier effective masses in the films were determined. It was found that the effective masses of conduction electrons in lonsdaleite films are lower than the effective masses of electrons in bulk case and asymptotically approach the bulk case effective masses as the film thickness increases.

Hydrogenated graphene can be considered as periodically connected cyclohexane carbon rings. Therefore, the conformers of cyclohexane dictate the conformers of graphane. The cyclohexane conformer "boat" corresponds to two graphane conformers: "boat1"[18] ("bed",[19] "boat",[20,21] see Figure 1a) and "boat2"[18] ("armchair",[21] see Figure 1b), whereas the conformer "chair" corresponds to graphane conformer "chair1"[18] (also called just "chair", see Figure 1c) and "chair2"[18]("washboard",[19] "stirrup",[20] "zigzag"[21]).

All of these graphane conformers can be considered as first members of the sp^3-hybridized film families with various crystallographic surface orientations. In particular, conformers "boat1" and "boat2" are the first members of lonsdaleite-type films with $(10\bar{1}0)$ (Figure 1d) and $(\bar{2}110)$ (Figure 1e) surfaces, respectively. Graphane conformer "chair1" belongs to both the group of diamond films with (111) surface and the group of lonsdaleite films with (0001) surface depending on how its graphene layers are stacked (Figure 1f). Multilayered graphene could have AA′, AA, AB, or ABC stacking with nearly the same energy,[22] as shown experimentally.[23−25] AA′ stacking of multilayered graphene forms the intermediate state between AA and AB types of stacking, where the graphene planes are translated by a half width of the hexagon and can form together with AA stacked graphene.[22,26] The chemical connection of AA′ graphene layers leads to the formation of lonsdaleite films with $(10\bar{1}0)$ surface, whereas AA stacking is the base for the formation of $(\bar{2}110)$ and (0001) films.

First, the stability of the lonsdaleite films was analyzed. The structure of sp^3-hybridized nanoclusters was exposed to surface effects that cause the graphitization process or the transformation of the outer carbon layers to graphene. This process was directly observed in diamond nanoclusters[27] and nanowires[28] and can play a major role in the stability of the considered films due to their atomic thickness.

It was found that among the films with clean $(10\bar{1}0)$ surfaces with thicknesses from 2.86 (two layers) to 17.92 Å (nine layers), only the thinnest film is unstable and splits to bilayered graphene. Investigation of the films with $(\bar{2}110)$ surface shows that such structures are not susceptible to graphitization and even bilayered lonsdaleite film is stable.

Lonsdaleite films with clean (0001) surface are the most exposed to graphitization. These films become stable only when they are thicker than 10.8 Å (six layers), but the outer layers split into graphene. This significantly differs from the case of diamond films with (111) surface where only films with thickness <8.42 Å (five layers) are unstable.[29]

The appearance of lonsdaleite structures as stacking faults or twin boundaries in diamond can be considered as lonsdaleite films implemented into diamond matrix. The possibility of isolating such a quasi-2-D object is intriguing, but available experimental data[30] prevent the expectation of fabricating lonsdaleite films from bulk diamond. However, known "bottom-up" paradigm allows the fabrication of lonsdaleite structures from smaller objects such as graphene. The number of theoretical predictions[8−10] and experimental observations[11−13] of the diamondization of multilayered graphene allows us to assume that freestanding lonsdaleite films could be fabricated through the chemical connection of neighbored carbon layers in the stack.

Graphene films can be transformed to lonsdaleite films by applying direct pressure. The amount of pressure needed can

dx.doi.org/10.1021/jz402528q | J. Phys. Chem. Lett. 2014, 5, 541−548

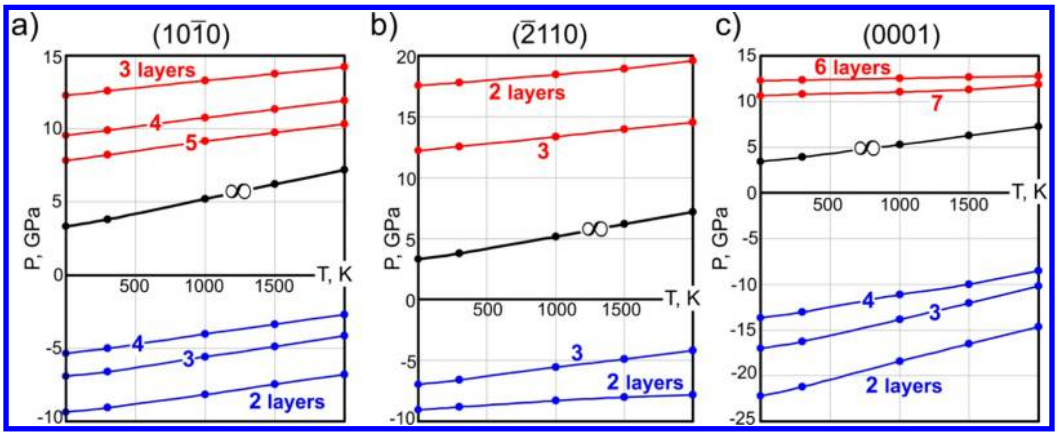

Figure 2. Phase diagram $P(T)$ of the phase transitions from multilayered graphene to lonsdaleite film with (a) (10$\bar{1}$0)surface, (b) ($\bar{2}$110) surface, and (c) (0001) surface for different number of layers (different thickness). Red and blue lines represent phase boundaries between multilayered graphene and lonsdaleite films with clean and hydrogenated surfaces, respectively. Every line is marked by the quantity of carbon layers in the structure; the bulk case is marked by an infinity sign. The phase of the multilayered graphene (graphite in limited case) is located under each line, and the phases of lonsdaleite films (bulk lonsdaleite in limited case) are arranged over each line.

be evaluated by taking the difference between the free energies of multilayered graphene and lonsdaleite film and dividing by the difference between atomic volumes of graphite and bulk lonsdaleite.

We obtained a phase diagram of such transitions in the temperature range 0−2000 K, as shown in the Figure 2 by red lines. The obtained phase diagrams allow the estimation of the fabrication conditions for lonsdaleite films from multilayered graphene. In the experimental paper,[13] the formation of sp^3 bonds between layers of seven-layered graphene at 16 GPa was reported. This high value agrees with our estimations that seven-layered graphene film should transit to lonsdaleite film with (0001) surface at 12 GPa (300 K); see Figure 2c.

The large phase transition pressure for the considered lonsdaleite films makes the formation process difficult and means the process requires the presence of a catalyst. The role of the catalyst can be played by the hydrogen adatoms on the surface of multilayered graphene. The binding of hydrogen atoms to the surface of multilayered graphene leads to the transformation of a practically chemically inert sp^2-hybridized carbon lattice to a semihydrogenated sp^3-hybridized film named graphone.[31] This material is highly strained and unstable due to the unpaired electrons of carbon atoms not bounded with hydrogen.[32] The formed graphone layer tends to compensate the dangling bonds by connection with the underlying graphene layer to form two-layered sp^3-hybridized carbon film. The sp^3-hybridized carbon atoms of the second layer also tend to connect with the next graphene layer and so on. The same story takes place from the bottom side of the multilayered graphene, and thus these processes go toward each other from the top to the bottom and vice versa. It was shown that such a process occurs without any activation barrier for the nanometer-sized films.[9,14]

The comparison between the free energies of hydrogenated lonsdaleite film and multilayered graphene with adsorbed hydrogen atoms on the surface showed that the pressure of such a phase transition is formally below zero. This originated from the fact that binding energy of the graphene with the adsorbed hydrogen atoms on the surfaces is lower than the binding energy of the corresponding lonsdaleite film.

The feasibility of the proposed method is justified by available experimental data on the diamondization of multilayered graphene[12] and amorphous carbon[33] induced by hydrogenation. Other types of surface functionalization can be used instead of hydrogen as well. This was illustrated by experimental reports of the connection of graphene layers to diamond film by the chemical adsorption of hydroxyl groups[11] and fluorine.[34]

Different organizations of adatoms on the graphene surface could lead to the formation of every graphane conformer considered in the paper and the formation of lonsdaleite films with (10$\bar{1}$0), ($\bar{2}$110), and (0001) surfaces. Therefore, the control over the organization of adsorbed atoms onto the graphene surface is critical in this issue and can depend on the adatom's type and upon external conditions.

Reference 19 supposes that the structure of the graphane/fluorographene surface can contain several phases divided by grain boundary. In the case of thicker lonsdaleite films, such a situation cannot be realized due to the high lattice strain caused by neighboring different crystallographically oriented surfaces with different symmetry and lattice parameters. It can be supposed that once formed, one type of surface in one region will propagate to the whole film structure.

We then investigated in detail the elastic properties of the lonsdaleite films. First, we estimated the 2-D elastic moduli for lonsdaleite films with (10$\bar{1}$0), ($\bar{2}$110), and (0001) surfaces and diamond film with (111) surface by defining the stress tensor due to strain as $\sigma_i = C_{ij}\eta_j$. This tensor corresponds to in-plane isotropic linear elasticity. We neglect the ambiguous thickness of 2D films; therefore, the dimension of the elastic modulus is N/m. We obtained the stress−strain, $\sigma_1-\eta_j$, relationships by simulating the uniaxial strains in the armchair (η_1) and zigzag (η_2) directions (Figure 1). These relationships allow us to estimate the values of the elastic constants C_{11}' and C_{12}', respectively. It should be noted that the elastic constants calculated for films of different symmetry relate to different constants of lonsdaleite crystal (Table 1). From Table 1, we can assume that films with the surface (10$\bar{1}$0) should display the highest values of C_{11}' and C_{12}'. Films with ($\bar{2}$110) and (0001) surfaces should display lower values. The values should approach each other as the film's thickness increases. Calculated data support this assumption (Figure 3a). Additionally, the comparison between the $C_{11}'$and C_{12}'constants of lonsdaleite

dx.doi.org/10.1021/jz402528q | J. Phys. Chem. Lett. 2014, 5, 541−548

Table 1. Relation between the Two-Dimensional Elastic Constants of Lonsdaleite Films with Different Crystallographic Orientation of Surfaces[a]

	$(10\bar{1}0)$	$(\bar{2}110)$	(0001)
C_{11}'	C_{33}	C_{11}	C_{11}
C_{12}'	C_{13}	C_{13}	C_{12}

[a]Corresponding bulk constants (from the ref 35): C_{11} = 1222.5 GPa, C_{12} = 106.8 GPa, C_{13} = 47.5 GPa, C_{33} = 1326.3 GPa, and C_{44} = 459.4 GPa.

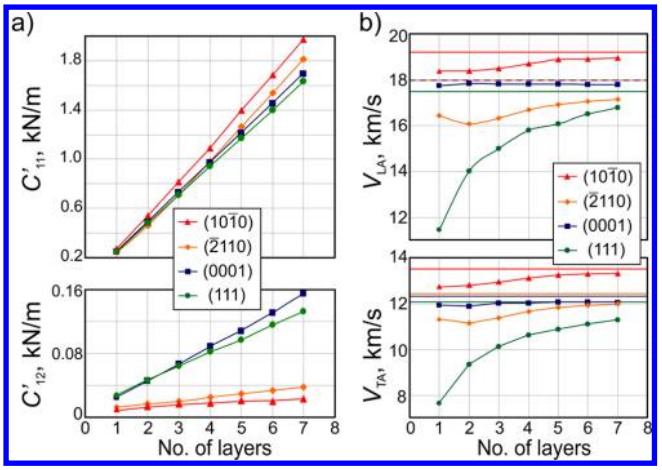

Figure 3. Dependence of the (a) elastic constants C_{11}', C_{12}' and (b) velocities of longitudinal ν_{LA} and transverse ν_{TA} acoustic waves of the lonsdaleite films with $(10\bar{1}0)$ (▲), $(\bar{2}110)$ (◆), and (0001) (■) surfaces for different number of layers (different thickness) in comparison with diamond films with (111) surface (●).

and diamond films with the same thickness shows that lonsdaleite films are stiffer than the diamond films.

From the obtained elastic constants, the velocities of longitudinal and transverse acoustic waves can be estimated using the following relations: $\nu_{LA} = (C_{11}'/\rho_{2D})^{1/2}$ and $\nu_{TA} = ((1/2(C_{11}' - C_{12}')/\rho_{2D})^{1/2}$, where ρ_{2D} is the formal 2-D density (kg/m^2 units). Such valuable characteristics could be compared with the corresponding data of bulk diamond and lonsdaleite. It was shown that lonsdaleite films display higher values not only compared with diamond film but also when compared with all known solids except bulk lonsdaleite and graphene. It is also clearly seen that acoustic velocities increased with increasing film thickness and that the velocities asymptotically approached corresponding bulk values (Figure 3b).

Another important mechanical characteristic of carbon films is behavior under critical deformation. In experiments, the 2-D films are usually probed by indenting the center of each freestanding film with the tip of an atomic force microscope.[36,37] We simulated this process using an empirical interatomic bond-order Brenner potential because of the large size (10^4 to 4×10^4 atoms) of the considered structures. The chosen approach is justified by successful application of the potential in numerous studies of elastic properties of graphene[38] and diamond films.[8]

The investigated lonsdaleite films had an equal radius (75 Å) with fastened edges, while the radius of the tip was nearly 10 times smaller than that in the experimental setup.[36,37] Deflection was carried out with a step of 0.2 Å. At each step, the system was relaxed using conjugated gradient minimization.

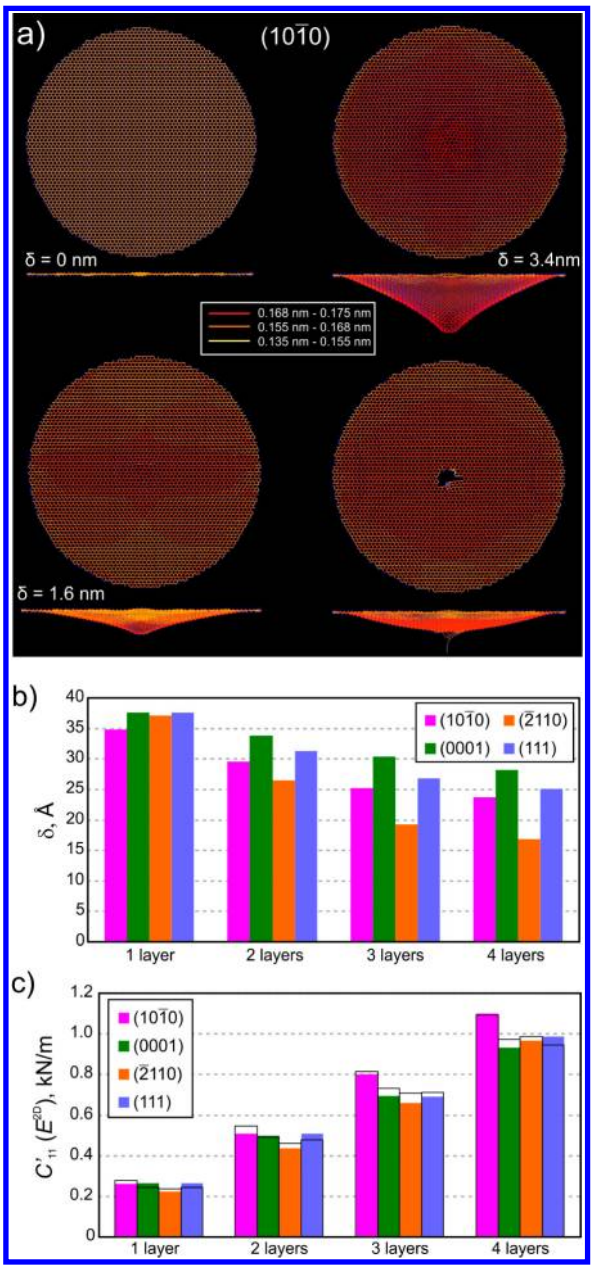

Figure 4. (a) Deformation sequence for lonsdaleite films with $(10\bar{1}0)$ surface: unloaded structure, with indentation depth δ = 1.6 nm, δ = 3.4 nm (critical strain), and after the failure. The color variation represents the bond lengths, from red (0.168 to 0.175 nm) to yellow (0.135 to 0.155 nm). (b) Dependence of the critical deflection upon the films thickness. (c) Dependence of E^{2D} (solid bars) upon the film thickness for all types of crystallographic surfaces in comparison with corresponding elastic constant C_{11}' (open bars) calculated by DFT.

The pressure induced by the tip causes the C−C bonds to elongate as displayed by color gradient (see Figure 4a for single layered film with $(10\bar{1}0)$ surface and Figure S1 in the Supporting Information for other studied films). The distribution of the strained bonds was directly related to the symmetry of the films. We plotted the dependence of critical deflection value (where films are punctured in the center, Figure 4a) upon the thickness of the films (Figure 4b). It was found that as their thickness increases, films become stiffer and more brittle. Surprisingly though, even four-layered films display very high elasticity, with a critical indentation depth

dx.doi.org/10.1021/jz402528q | J. Phys. Chem. Lett. 2014, 5, 541−548

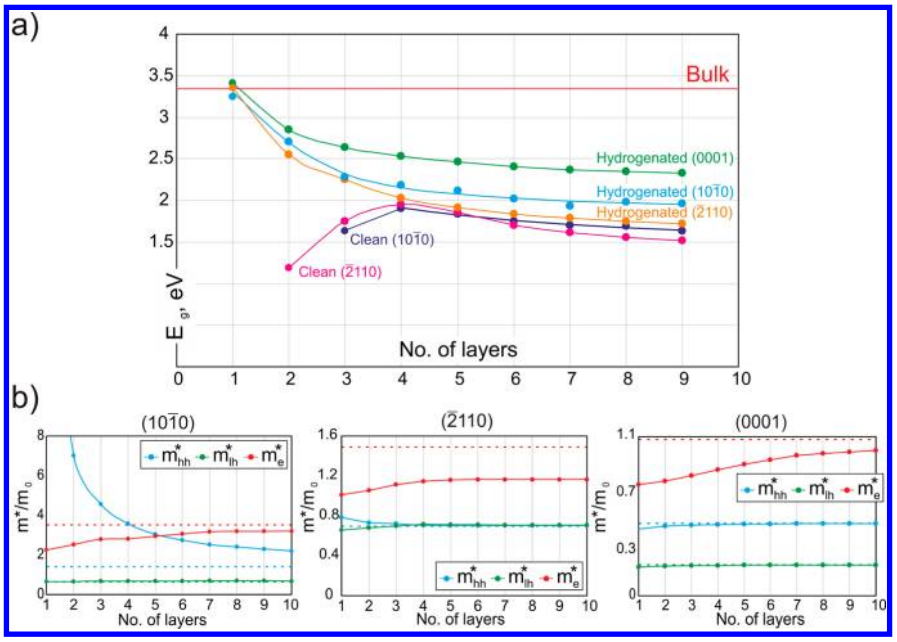

Figure 5. (a) Band gap dependence of the lonsdaleite films with (10$\bar{1}$0), ($\bar{2}$110), and (0001) surfaces based upon the number of layers (thickness). (b) Dependence of the effective masses of electrons and holes on the number of layers along the main directions of symmetry for films with (10$\bar{1}$0), ($\bar{2}$110) surfaces ($\Gamma \rightarrow Y$ direction) and with (0001) surface ($\Gamma \rightarrow M$ direction).

only 1.5 ((10$\bar{1}$0) surface), 2.2 (($\bar{2}$110) surface), and 1.4 ((0001) surface) times smaller than that of their corresponding monolayered structures. The same results were obtained for the diamond films with (111) surface.

The obtained dependence of the strain energy E of the carbon sheet upon the deflection was fitted by the fourth-order polynomial $E(\delta) = \sigma^{2D}(\pi a)(\delta^2/2a) + E^{2D}(q^3a)(\delta^4/4a^3) + E_0$, which is the integrated equation for the force used in experimental works.[36,37] Here σ^{2D} is the pretension of the film, a is the radius of the structure, δ is the deflection of the atom in the center point, E^{2D} is the stiffness coefficient, and $q = 1/(1.05 - 0.15\nu - 0.16\nu^2)$, where $\nu = 0.2$ is the Poisson coefficient for diamond.[30] It was found that E^{2D} values increase almost linearly with film thickness (Figure 4c). This coefficient is directly related to the C_{11}' modulus,[37,39] which allows us to compare the estimations by classical Brenner potential with DFT calculations; see Figure 4c. The close correspondence of two sets of data validates the chosen approaches and allows the conclusion that the considered structures display the highest stiffness and flexibility.

Finally, we considered the electronic properties of the studied films. The band structures of the different graphane conformers and corresponding types of lonsdaleite films are similar and display semiconducting behavior. The band gap width dependence of hydrogenated films with (10$\bar{1}$0), ($\bar{2}$110), and (0001) surfaces and films with nonpassivated clean (10$\bar{1}$0), ($\bar{2}$110) surfaces upon the number of layers are shown in Figure 5a. All graphane conformers show closely adjacent band gap values around 3.25 eV. The band gaps of the films are lower than the band gaps of both graphane and bulk lonsdaleite (3.35 eV), which is evidence of the existence of a minimum in the band gap function of the film thickness. This nonlinear behavior can be explained by surface states and the quantum confinement effect.[9,17] As the film thickness increases, the surface contribution to the electronic structure decreases. This leads to band gap augmentation due to an increase in the bulk contribution. All hydrogenated films display direct band gap, which allows us to assume the structures have applications in nanoelectronics and nanooptics, for example, use as an active laser medium. Films with clean surfaces display an additional extreme point in the width of the band gap function when the number of layers corresponded to four-layered films (Figure 5a). This extremum is related to the transition from direct band gap to indirect band gap.

One of the most important characteristics of semiconducting material is the effective mass of its carriers. The effective masses $m^* = \hbar^2(\partial^2E/\partial k^2)^{-1}$ of both electrons and holes along the main directions of symmetry for lonsdaleite films with different thicknesses were determined and are shown in Figure 5b. It was found that the electron effective masses of the films are lower than corresponding masses in bulk lonsdaleite, which allows us to assume that there is better electronic transport in such structures. In the case of films with (10$\bar{1}$0) surface, only electrons have effective masses lower than those in the bulk case. Heavy holes display much larger values for the thinnest films than holes in bulk lonsdaleite, and the effective masses decrease with increasing thickness nearly exponentially. The effective masses of heavy and light holes of hydrogenated lonsdaleite films with ($\bar{2}$110) surface along the $\Gamma \rightarrow Y$ direction degenerate with increasing thickness and approach $0.695m_0$, which corresponds to the effective mass of the hole in lonsdaleite for the corresponding symmetry direction. Heavy and light holes of hydrogenated lonsdaleite films with (0001) surface demonstrate behavior practically independent of the thickness.

Lonsdaleite films with nanometer thickness were investigated for the first time. We discussed the stability of these films and estimated the phase diagram $P(T)$ for the transition from multilayered graphene to lonsdaleite film. Additionally, we studied the effect of chemically induced phase transition when lonsdaleite film forms from the multilayered graphene by chemical adsorption of hydrogen adatoms to the surface and extend the phase diagram for this case. We investigated the elastic and electronic properties of the lonsdaleite films. We

dx.doi.org/10.1021/jz402528q | J. Phys. Chem. Lett. 2014, 5, 541−548

found that values of the elastic constants and the acoustic velocities of lonsdaleite films are higher than those for diamond films with the same thickness. This makes lonsdaleite films second in stiffness only to the bulk lonsdaleite and graphene. It was found that investigated films are highly flexible. The films display peculiar band structure with direct band gap and nonlinear behavior of the relation between its band gap width and the films thickness. It was found that the effective masses of conduction electrons of the films are lower than the corresponding masses in bulk lonsdaleite, which allows us to assume better electronic transport in such structures. The combination of the obtained properties makes quasi-2-D lonsdaleite films a promising material for electronic, chemical sensing, and optical applications as the thinnest semiconducting films with extremely high stiffness. This makes further investigations of sp^3-hybridized carbon films particularly intriguing.

COMPUTATIONAL DETAILS

All calculations of the atomic structure and electronic properties were performed using density functional theory (DFT)[40,41] in the generalized gradient approximation with the Perdew–Burke–Ernzerhof (PBE) exchange correlation functional,[42] as implemented into the VASP[43−45] package. The plane-wave energy cutoff was set to 500 eV, while the Brillouin zone was sampled using an 8 × 8 × 1 Monkhorst–Pack grid.[46] Atomic structure optimization was carried out when the maximum interatomic force became <0.01 eV/Å. The effective masses of both electrons and holes were determined using a k-point spacing smaller than 0.01 $Å^{-1}$. To avoid interaction between the neighboring diamond or graphene layers, we set the translation vector along the c axis of the hexagonal supercells to be >15 Å.

To evaluate the accuracy of the chosen approach, we calculated and compared the atomic geometry and electronic and elastic properties of graphene and bulk diamond with corresponding experimental values. It was found that the DFT-PBE method predicts the structural parameters of a considered systems with an error <0.05% (compared with the experimental data for diamond taken from[47] a_{calc} = 3.566 Å and a_{exp} = 3.568 Å and for graphene taken from[48] a_{calc} = 2.469 Å and a_{exp} = 2.459 Å). The bulk modulus of the diamond was determined as B = 432 GPa, which is in good agreement with the reference values (B = 442 GPa[49]). The electronic band gap of diamond was evaluated to be E_g = 4.5 eV, which is lower than the experimental value (5.45 eV[30]) due to a systematic underestimation of band gap by DFT-PBE.

The phase diagram was also performed at a DFT level of theory in a local density approximation using the Perdew–Zunger parametrization[40,50] and a plane-wave basis set using Quantum ESPRESSO package.[51] The plane-wave energy cutoff was 30 Ry.

The phase diagram was obtained from the calculation of the Gibbs free energies G of the compared phases in the quasi-harmonic approximation:[52]

$$G(P, T) = E_0(V) + PV + U_0(V) + F_{vib}(T, V)$$

where E_0 is the total energy from the DFT calculations and U_0 and F_{vib} are the zero-point and vibrational energies calculated from the following relations:

$$U_0(V) = \frac{1}{2}\int g(V, \omega)\hbar\omega \, d\omega$$

$$F_{vib}(T, V) = k_B T \int_\Omega g(V, \omega) \ln\left[1 - \exp\left(-\frac{\hbar\omega}{k_B T}\right)\right] d\omega$$

Here $g(\omega(P))$ is the phonon density of states at the given pressure, calculated using density functional perturbation theory.[53] After phonon density of states integration, zero-point and vibrational energies (for each chosen temperature) were calculated from the corresponding relations. Substitution of all calculated energy contributions into the equation for Gibbs free energy allows us to obtain the temperature-dependent phase transition pressure value. The chosen approach is validated by a number of reference papers[52,54] that calculated the phase diagram $P(T)$ of various materials.

The behavior of the films under critical strain was simulated in the framework of classical molecular dynamics with Brenner potential[55] implemented into LAMMPS package.[56]

ASSOCIATED CONTENT

Supporting Information

Deformation sequence for lonsdaleite films with $(10\bar{1}0)$, (0001), and $(\bar{2}110)$ surfaces. This material is available free of charge via the Internet at http://pubs.acs.org.

AUTHOR INFORMATION

Corresponding Author

*E-mail: agkvashnin@gmail.com.

Notes

The authors declare no competing financial interest.

ACKNOWLEDGMENTS

We are grateful to the Moscow State University for use of the cluster computers 'Chebishev' and 'Lomonosov'. This work was supported by the Ministry of Education and Science of the Russian Federation (Contract No. 14.B37.21.1645). A.G.K. acknowledges the support from Scholarship of President of Russia for young scientists and Ph.D. students (competition SP-2013). P.B.S. acknowledges the support from the Ministry for Education and Science of the Russian Federation (Project No. 11.G34.31.0061) and the Russian Foundation for Basic Research (project no. 12-02-31261).

REFERENCES

(1) Foote, A. E. A New Locality for Meteoritic Iron with a Preliminary Notice of the Discovery of Diamonds in the Iron. *Am. J. Sci.* **1891**, *42*, 413−417.

(2) Frondel, C.; Marvin, U. B. Lonsdaleite, a Hexagonal Polymorph of Diamond. *Nature* **1967**, *214*, 587−589.

(3) Kurdyumov, A. V.; Slesarev, V. N.; Ostrovskaya, N. F.; Golubev, A. S.; Dubitskii, G. A.; Pilipenko, V. A. Structural Features and Mechanism of Formation of Lonsdaleite. *Dokl. Akad. Nauk SSSR* **1980**, *255*, 1382−1385.

(4) Britun, V. F.; Kurdyumov, A. V.; Petrusha, I. A. Diffusionless Nucleation of Lonsdaleite and Diamond in Hexagonal Graphite under Static Compression. *Powder Metall. Met. Ceram.* **2004**, *43*, 87−93.

(5) Kulnitskiy, B.; Perezhogin, I.; Dubitsky, G.; Blank, V. Polytypes and Twins in the Diamond-Lonsdaleite System Formed by High-Pressure and High-Temperature Treatment of Graphite. *Acta Crystallogr., Sect. B: Struct. Sci* **2013**, *69*, 474−479.

(6) Denisov, V. N.; Mavrin, B. N.; Serebryanaya, N. R.; Dubitsky, G. A.; Aksenenkov, V. V.; Kirichenko, A. N.; Kuzmin, N. V.; Kulnitskiy, B. A.; Perezhogin, I. A.; Blank, V. D. First-principles, UV Raman, X-ray Diffraction and TEM Study of the Structure and Lattice Dynamics of the Diamond−Lonsdaleite System. *Diamond Relat. Mater.* **2011**, *20*, 951−953.

(7) Pan, Z.; Sun, H.; Zhang, Y.; Chen, C. Harder Than Diamond: Superior Indentation Strength of Wurtzite BN and Lonsdaleite. *Phys. Rev. Lett.* **2009**, *102*, 055503.
(8) Chernozatonskii, L. A.; Sorokin, P. B.; Kvashnin, A. G.; Kvashnin, D. G. Diamond-like C_2H Nanolayer, Diamane: Simulation of the Structure and Properties. *JETP Lett.* **2009**, *90*, 134−138.
(9) Zhu, L.; Hu, H.; Chen, Q.; Wang, S.; Wang, J.; Ding, F. Formation and Electronic Properties of Hydrogenated Few Layer Graphene. *Nanotechnology* **2011**, *22*, 185202.
(10) Leenaerts, O.; Partoens, B.; Peeters, F. M. Hydrogenation of Bilayer Graphene and the Formation of Bilayer Graphane from First Principles. *Phys. Rev. B* **2009**, *80*, 245422.
(11) Barboza, A. P. M.; Guimaraes, M. H. D.; Massote, D. V. P.; Campos, L. C.; Neto, N. M. B.; Cancado, L. G.; Lacerda, R. G.; Chacham, H.; Mazzoni, M. S. C.; Neves, B. R. A.; et al. Room-temperature Compression-induced Diamondization of Few-layer Graphene. *Adv. Mater.* **2011**, *23*, 3014−3017.
(12) Rajasekaran, S.; Abild-Pedersen, F.; Ogasawara, H.; Nilsson, A.; Kaya, S. Interlayer Carbon Bond Formation Induced by Hydrogen Adsorption in Few-layer Supported Graphene. *Phys. Rev. Lett.* **2013**, *111*, 085503.
(13) Clark, S.; Jeon, K. J.; Chen, J. Y.; Yoo, C. S. Few-layer Graphene under High Pressure: Raman and X-ray Diffraction Studies. *Solid State Commun.* **2012**, *154*, 15−18.
(14) Kvashnin, A. G.; Chernozatonskii, L. A.; Yakobson, B. I.; Sorokin, P. B. Phase Diagram of Quasi-2-dimensional Carbon, from Graphene to Diamond. *Nano Lett.* **2014**, DOI: 10.1021/nl403938g.
(15) Fyta, M. Nitrogen-vacancy Centers and Dopants in Ultrathin Diamond Films: Electronic Structure. *J. Phys. Chem. C* **2013**, *117*, 21376−21381.
(16) Hu, C. H.; Zhang, P.; Liu, H. Y.; Wu, S. Q.; Yang, Y.; Zhu, Z. Z. Structural Stability and Electronic and Magnetic Properties of Fluorinated Bilayer Graphene. *J. Phys. Chem. C* **2013**, *117*, 3572−3579.
(17) Chernozatonskii, L. A.; Sorokin, P. B.; Kuzubov, A. A.; Sorokin, B. P.; Kvashnin, A. G.; Kvashnin, D. G.; Avramov, P. V.; Yakobson, B. I. Influence of Size Effect on the Electronic and Elastic Properties of Diamond Films with Nanometer Thickness. *J. Phys. Chem. C* **2011**, *115*, 132−136.
(18) Wen, X. D.; Hand, L.; Labet, V.; Yang, T.; Hoffmann, R.; Ashcroft, N. W.; Oganov, A. R.; Lyakhov, A. O. Graphane Sheets and Crystals under Pressure. *Proc. Natl. Acad. Sci.* **2011**, *108*, 6833−6837.
(19) Artyukhov, V. I.; Chernozatonskii, L. A. Structure and Layer Interaction in Carbon Monofluoride and Graphane: a Comparative Computational Study. *J. Phys. Chem. A* **2010**, *114*, 5389−5396.
(20) Bhattacharya, A.; Bhattacharya, S.; Majumder, C.; Das, G. P. Third Conformer of Graphane: a First-Principles Density Functional Theory Study. *Phys. Rev. B* **2011**, *83*, 033404.
(21) Leenaerts, O.; Peelaers, H.; Hernández-Nieves, A. D.; Partoens, B.; Peeters, F. M. First-Principles Investigation of Graphene Fluoride and Graphane. *Phys. Rev. B* **2010**, *82*, 195436.
(22) Lee, J. K.; Lee, S. C.; Ahn, J. P.; Kim, S. C.; Wilson, J. I. B.; John, P. The Growth of AA Graphite on (111) Diamond. *J. Chem. Phys.* **2008**, *129*, 234709.
(23) Lui, C. H.; Li, Z.; Mak, K.; Cappelluti, E.; Heinz, T. F. Observation of an Electrically Tunable Band Gap in Trilayer Graphene. *Nat. Phys.* **2011**, *7*, 944−947.
(24) Cong, C.; Yu, T.; Sato, K.; Shang, J.; Saito, R.; Dresselhaus, G. F.; Dresselhaus, M. S. Raman Characterization of ABA- and ABC-stacked Trilayer Graphene. *ACS Nano* **2011**, *5*, 8760−8768.
(25) Liu, Z.; Suenaga, K.; Harris, P. J. F.; Iijima, S. Open and Closed Edges of Graphene Layers. *Phys. Rev. Lett.* **2009**, *102*, 015501.
(26) Lee, J. K.; Lee, S.; Kim, Y. I.; Kim, J. G.; Lee, K. I.; Ahn, J. P.; Min, B. K.; Yu, C. J.; Chae, K. H.; John, P.; et al. Structure of Multi-Wall Carbon Nanotubes: AA′ Stacked Graphene Helices. *Appl. Phys. Lett.* **2013**, *102*, 161911.
(27) Kuznetsov, V. L.; Butenko, Y. V. Nanodiamond Graphitization and Properties of Onion-like Carbon. In *Synthesis, Properties and Applications of Ultrananocrystalline Diamond*; Springer: Dordrecht, The Netherlands, 2005; Vol. *192*, pp 199−216.
(28) Shang, N.; Papakonstantinou, P.; Wang, P.; Zakharov, A.; Palnitkar, U.; Lin, I. N.; Chu, M.; Stamboulis, A. Self-assembled Growth, Microstructure, and Field-Emission High-performance of Ultrathin Diamond Nanorods. *ACS Nano* **2009**, *3*, 1032−1038.
(29) Li, H.; Li, J.; Wang, Z.; Zou, G. Layer Number-Dependent Structural Evolution of Two-Dimensional Diamond Films. *Chem. Phys. Lett.* **2012**, *550*, 130−133.
(30) Spear, K. E.; Dismukes, J. P. *Synthetic Diamond: Emerging CVD Science and Technology*; Wiley: New York, 1994.
(31) Zhou, J.; Wang, Q.; Sun, Q.; Chen, X. S.; Kawazoe, Y.; Jena, P. Ferromagnetism in Semihydrogenated Graphene Sheet. *Nano Lett.* **2009**, *9*, 3867−3870.
(32) Podlivaev, A. I.; Openov, L. A. On the Thermal Stability of Graphone. *Semiconductors* **2011**, *45*, 958−961.
(33) Lifshitz, Y.; Kohler, T.; Frauenheim, T.; Guzmann, I.; Hoffman, A.; Zhang, R. Q.; Zhou, X. T.; Lee, S. T. The Mechanism of Diamond Nucleation from Energetic Species. *Science* **2002**, *297*, 1531−1533.
(34) Watanabe, N. Two Types of Graphite Fluorides, $(CF)_n$ and $(C_2F)_n$, and Discharge Characteristics and Mechanisms of Electrodes of $(CF)_n$ and $(C_2F)_n$ in Lithium Batteries. *Solid State Ionics* **1980**, *1*, 87−110.
(35) Wang, S. Q.; Ye, H. Q. Ab-initio Elastic Constants for the Lonsdaleite Phases of C, Si and Ge. *J. Phys.: Condens. Matter* **2003**, *15*, 5307−5314.
(36) Lee, C.; Wei, X.; Kysar, J. W.; Hone, J. Measurement of the Elastic Properties and Intrinsic Strength of Monolayer Graphene. *Science* **2008**, *321*, 385−388.
(37) Song, L.; Ci, L.; Lu, H.; Sorokin, P. B.; Jin, C.; Ni, J.; Kvashnin, A. G.; Kvashnin, D. G.; Lou, J.; Yakobson, B. I.; et al. Large Scale Growth and Characterization of Atomic Hexagonal Boron Nitride Layers. *Nano Lett.* **2010**, *10*, 3209−3215.
(38) Zhao, H.; Min, K.; Aluru, N. R. Size and Chirality Dependent Elastic Properties of Graphene Nanoribbons Under Uniaxial Tension. *Nano Lett.* **2009**, *9*, 3012−3015.
(39) Kudin, K. N.; Scuseria, G. E.; Yakobson, B. I. C_2F, BN, and C Nanoshell Elasticity from Ab Initio Computations. *Phys. Rev. B* **2001**, *64*, 235406.
(40) Hohenberg, P.; Kohn, W. Inhomogeneous Electron Gas. *Phys. Rev.* **1964**, *136*, B864.
(41) Kohn, W.; Sham, L. J. Self-consistent Equations Including Exchange and Correlation Effects. *Phys. Rev. B* **1965**, *140*, A1133−A1138.
(42) Perdew, J. P.; Burke, K.; Ernzerhof, M. Generalized Gradient Approximation Made Simple. *Phys. Rev. Lett.* **1996**, *78*, 3865−3868.
(43) Kresse, G.; Hafner, J. Ab Initio Molecular Dynamics for Liquid Metals. *Phys. Rev. B* **1993**, *47*, 558−561.
(44) Kresse, G.; Hafner, J. Ab Initio Molecular-Dynamics Simulation of the Liquid-Metal-Amorphous-Semiconductor Transition in Germanium. *Phys. Rev. B* **1994**, *49*, 14251−14269.
(45) Kresse, G.; Furthmüller, J. Efficient Iterative Schemes for Ab Initio Total-Energy Calculations Using a Plane-Wave Basis Set. *Phys. Rev. B* **1996**, *54*, 11169−11186.
(46) Monkhorst, H. J.; Pack, J. D. Special Points for Brillouin-zone Integrations. *Phys. Rev. B* **1976**, *13*, 5188−5192.
(47) Wyckoff, R. W. G. *Crystal Structures*, 2nd ed.; Interscience Publishers: New York, 1963.
(48) Baskin, Y.; Meyer, L. Lattice Constants of Graphite at Low Temperatures. *Phys. Rev.* **1955**, *100*, 544.
(49) Cohen, M. L. Calculation of Bulk Moduli of Diamond and Zinc-blende Solids. *Phys. Rev. B* **1985**, *32*, 7988−7991.
(50) Perdew, J.; Zunger, A. Self-interaction Correction to Density-Functional Approximations for Many-Electron Systems. *Phys. Rev. B* **1981**, *23*, 5048−5079.
(51) Giannozzi, P.; Baroni, S.; Bonini, N.; Calandra, M.; Car, R.; Cavazzoni, C.; Ceresoli, D.; Chiarotti, G. L.; Cococcioni, M.; Dabo, I.; et al. Quantum Espresso: a Modular and Open-source Software Project for Quantum Simulations of Materials. *J. Phys.: Condens. Matter* **2009**, *21*, 395502.

(52) Kern, G.; Kresse, G.; Hafner, J. Ab Initio Calculation of the Lattice Dynamics and Phase Diagram of Boron Nitride. *Phys. Rev. B* **1999**, *59*, 8551−8559.
(53) Baroni, S.; de Gironcoli, S.; Dal Corso, A.; Giannozzi, P. Phonons and Related Crystal Properties from Density-Functional Perturbation Theory. *Rev. Mod. Phys.* **2001**, *73*, 515−562.
(54) Luo, W.; Windl, W. First Principles Study of the Structure and Stability of Carbynes. *Carbon* **2009**, *47*, 367−383.
(55) Brenner, D.; Shenderova, O.; Harrison, J.; Stuart, S.; Ni, B.; Sinnott, S. A Second-generation Reactive Empirical Bond Order (REBO) Potential Energy Expression for Hydrocarbons. *J. Phys.: Condens. Matter* **2002**, *14*, 783−802.
(56) Plimpton, S. Fast Parallel Algorithms for Short-range Molecular Dynamics. *J. Comput. Phys.* **1995**, *117*, 1−19.